IEEE Access
Multidisciplinary | Rapid Review | Open Access Journal

Received August 11, 2021, accepted August 25, 2021, date of publication August 31, 2021, date of current version September 10, 2021.

Digital Object Identifier 10.1109/ACCESS.2021.3109420

Tunable 24-GHz Antenna Arrays Based on Nanocrystalline Graphite

M. ALDRIGO[1], (Member, IEEE), M. DRAGOMAN[1], S. IORDANESCU[1], (Life Member, IEEE), A. AVRAM[1], O.-G. SIMIONESCU[1,2], C. PARVULESCU[1], H. EL GHANNUDI[3], S. MONTORI[3], L. NICCHI[3], S. XAVIER[4], AND A. ZIAEI[4], (Member, IEEE)

[1]National Institute for Research and Development in Microtechnologies, IMT-Bucharest, 077190 Voluntari, Romania
[2]Doctoral School of Physics, University of Bucharest, 077125 Măgurele, Romania
[3]RF Microtech S.r.l., 06132 Perugia, Italy
[4]Thales Research and Technology France, Campus Polytechnique, 91767 Palaiseau, France

Corresponding author: M. Aldrigo (martino.aldrigo@imt.ro)

This work was supported in part by the European Project H2020 ICT-07-201 NANOSMART under Grant 825430, in part by the European Project H2020 FETOPEN-01-2018-2019-2020 NANOPOLY under Grant 829061, and in part by two grants of the Romanian Ministry of Research, Innovation and Digitalization, CCCDI-UEFISCDI, within PNCDI III, under Project PN-III-P3-3.6-H2020-2020-0073 and Project PN-III-P2-2.1-PTE-2019-0578.

ABSTRACT In this work, we present a tunable 24-GHz antenna array based on a CMOS-compatible 110-nm-thick nanocrystalline graphite film grown by plasma enhanced chemical vapor deposition. The film has a nominal bulk conductivity exceeding 16000 S/m (hence, greater than any graphene monolayer or industrially available graphene multilayer) but still able to show an outstanding modulation of its charge carrier density in the upper microwave spectrum. The manufactured layer was used to design, simulate, fabricate, and test a 24-GHz patch antenna array, with each radiating element having overall dimensions of just $\lambda_0/8 \times \lambda_0/7$. The fabricated array exhibits a measured maximum gain of about 3 dBi around 24 GHz (unbiased state), with a half-power beam width of only 14.5° (suitable in wireless links where a high directivity is envisaged). Spanning the dc bias voltage between -25 V and 25 V at 24 GHz, the gain can be tuned continuously between -1.5 dBi and 4 dBi, whereas the resonance frequency undergoes a maximum shift of 166 MHz. This voltage-dependent tuning of the gain represents a first step in developing carbon-based applications to control amplitude and phase simultaneously and independently. These results (never reported) demonstrate the big potential of nanocrystalline graphite for high-performance microwave components that are CMOS compatible (a highly desirable characteristic for high fabrication yield and large-scale production), with unprecedented tunability for next-generation high-capacity communications.

INDEX TERMS Carbon compounds, patch antennas, microwave antenna arrays, tuning.

I. INTRODUCTION

New communications systems (such as 5G and future 6G) require small and tunable high-frequency devices, since their backbone is the internet-of-things (IoT) that is a wireless network interconnecting tiny objects, e.g., sensors, actuators, and detectors. The antenna is a key component for such applications; therefore, it needs to be small and tunable to allow the accurate interconnection of hundreds, or even thousands, of ''things'' irrespective of propagation conditions. Hence, antennas based on two-dimensional (2D) materials, like graphene or MXenes, could be ideal candidates thanks to the fact that they are inherently tunable without any additional electronic circuits.

For a graphene monolayer, its surface impedance is $Z_s(\omega, V_b) = 1/\sigma(\omega, V_b) = R_s(\omega, V_b) + jX_s(\omega, V_b)$, where $\sigma(\omega, V_b)$ is graphene's conductivity and V_b is the external dc bias voltage. Since $\sigma(\omega, V_b)$ depends on a voltage (V_b) applied either vertically (in top gate and/or back-gate configuration, as in the case of graphene transistors) or as a lateral (i.e., in-plane) field across a slot, as in the case of graphene layers embedded with coplanar waveguides, the tunability of microwave scattering parameters can be achieved by the simple application of the proper dc voltage [1]. This inherent tunability is not valid only for graphene monolayers, but also for 2D multilayers in general [2], [3]. Up to now, ferromagnetics,

The associate editor coordinating the review of this manuscript and approving it for publication was Mahmoud A. Abdalla.

ferroelectrics, organic polymers, and liquid crystals have also demonstrated to confer an inherent tunability to microwave devices [4]–[6].

However, in the microwave range the surface resistance of graphene is in principle greater than few thousand ohms when no bias is applied, which is a detrimental effect for radiation (as it implies losses and a moderate efficiency). The origin of these phenomena can be found in the low surface conductivity of graphene, which is 10^{-4}–10^{-2} S·□ (Siemens·square) for monolayers [7], whereas metals have a bulk conductivity in the order of 10^6 S/m. There are many ways to increase the bulk conductivity of graphene composites up to 10^5–10^6 S/m [8]–[11] but, in these cases, for the obtained ''metal-like'' graphene antennas the dc electric field is not able to modulate such large electron densities to values comparable with metals [12], [13]; therefore, the main advantage of a 2D antenna (i.e., its inherent tunability) is lost to achieve good radiation efficiency and gain, as they would be obtained by any metal antenna or antenna array. As A. K. Geim noted: If not for graphene's high quality and tunability, there would be no new physics and, therefore, no graphene boom [14].

In this paper, we report on how to increase the conductivity of a carbon-based antenna without losing its inherent tunability, which is a major physical effect. In this respect, a nanocrystalline graphite (NCG) film was used, with a thickness of 110 nm (hence, much lower than the thickness of any metal used in microwaves, as it is necessary to avoid skin depth effect), grown on high-resistivity silicon/silicon oxide (HRSi/SiO_2) 4-inch wafers (for CMOS compatibility), and having a bulk conductivity of over 16000 S/m. This value is tens of times higher than that of a graphene monolayer (which has a surface conductivity in the order of 10^{-4} S·□, as stated before), but it is much lower compared to metals. Further, a 24-GHz patch antenna array was designed, simulated, fabricated, and tested using the proposed NCG/SiO_2/HRSi wafer to achieve a straightforward amplitude modulation of the radiated power (together with a moderate frequency tuning range), the phase change introduced by a complete beam forming network being out of the scope of this work. In deep contrast with graphene mono- or few-layer growth performed by chemical vapor deposition (CVD) on a metal and transferred onto the desired substrate (at the likely risk of creating wrinkles, cracks, and defects) [15], the NCG was grown directly by plasma enhanced chemical vapor deposition (PECVD) on the HRSi/SiO_2 substrate with a diameter of 100 mm [16]. The NCG exhibits a polycrystalline nature and consists in a network of graphite nanocrystals and grain boundaries. Depending on the size of these grain boundaries, the conductivity can be tuned from 10^2 S/m up to 10^4 S/m [17]. The outcome of the optimized PECVD process is a CMOS-compatible component (the antenna array) with a high fabrication yield, suitable for unprecedented large-scale production of carbon-based electronics. This represents a major improvement with respect to the patch antenna presented in [15], which relies on a graphene monolayer deposited on a ferroelectric thin film and exhibits a less pronounced gain tunability, together with a much lower radiation efficiency. Furthermore, at the industrial level it is not possible to grow thick (i.e., hundreds of nm) multilayer graphene at the wafer level using CVD, as it is fabricated via transfer, i.e., the graphene monolayers are first grown on copper and then piled up on the desired substrate. Therefore, the best that can be obtained so far is to transfer up to about 10 layers but no more than that. Even if the electrical conductivity increases with the number of layers, due to the nature of the transfer process the final samples have more impurities as one increases the number of layers. On the other hand, the proposed NCG films can be grown at any desired thickness with a high homogeneity and no impurities.

The manuscript is organized as follows. First, Section II provides a detailed description of the fabrication and physical/structural characterization of the NCG, to provide a set of experimental data for the accurate modelling of the material under test. Second, Section III describes the electromagnetic (EM) design of the single 24-GHz NCG-based patch antenna and of the entire 8-element linear array. Then, Section IV focuses on the fabrication of the proposed tunable array. Finally, Section V presents a comparison between simulations and microwave measurements, with a discussion about the results and the interpretation of the outcomes. Conclusions are given at the end of the paper, with future perspective for high-frequency applications of carbon-based antennas.

II. NCG THIN FILMS FABRICATION AND CHARACTERIZATION

The first step was the fabrication and physical/structural characterization of the NCG, as to provide useful data for the correct modelling of the material in the EM simulator used for the design of the antennas. The NCG deposition process was performed on the NANOFAB 1000 system (Oxford Instruments, UK), using the PECVD method [18]. The Si/SiO_2 wafer was loaded in the preheated reactor (200°C) and heated up to 900°C at a ramp rate of 15°C/min in an Ar+H_2 (5%) atmosphere. After reaching the target temperature, the process continued with a 10 min thermal pre-treatment step at 900°C in Ar+H_2 (5%) atmosphere, and a 5 min hydrogenation step in Ar+H_2 (10%). The NCG deposition was performed in CH_4+H_2 plasma (ratio 1:1.25) at 900°C, 100-W RF power and 1.5 Torr pressure, with a deposition rate of approximately 3 nm/min. After the deposition step was completed, the wafer was cooled down in the reactor to 200°C at a ramp rate of 9°C/min. After unloading from the reactor into the load lock chamber, the wafer was left to cool down for another 10 min in vacuum at 0.5 mTorr to reach room temperature before being exposed to atmosphere. To determine the type of deposited carbon thin film, Raman spectroscopy was performed using the LabRAM HR 800 (Horiba Jobin Yvon, Japan). The spectra were acquired at 633 nm and are presented in Fig. 1, whereas extracted parameters are presented in Table 1. One can notice the D band centered at ∼1350 cm^{-1} and the G band shifted from its

usual position (at 1580 cm^{-1}) to ∼1592 cm^{-1}. The D band/G band intensity peak ratio (I_D/I_G, which helps estimate the defects of a graphene or graphite sample) was calculated to be between 2.34 and 2.39, whereas the full width at half maximum (FWHM, which is an indication of the structural distribution and takes the effect of mean crystallite size and the size dispersion into account) was measured to be between 70 and 72 cm^{-1} for the D band and between 64 and 78 cm^{-1} for the G band. The blue shifting of the G band along with the I_D/I_G ratio in the 1.5–2.5 interval indicates the presence of a nanocrystalline graphite film [19]. From Fig. 1, the 2D peak can be also observed around 2700 cm^{-1}, which was expected due to the growth temperature of 900°C [20]. The surface roughness (RMS value) for the deposited NCG thin films was measured using the NTEGRA Aura (NT-MDT Co., Russia) atomic force microscopy system (AFM) on an area of 1 μm × 1 μm. For reference, the NCG roughness was compared to a bare Si wafer and to a SiO_2 thin film. In detail, the RMS roughness is 0.15 nm for bare Si, 1.13 nm for Si/SiO_2, 3.5 nm for Si/NCG and 3.7 nm for Si/SiO_2/NCG. From these comparative measurements we inferred that there is no significant difference between NCG thin films grown directly on Si or Si/SiO_2 substrates.

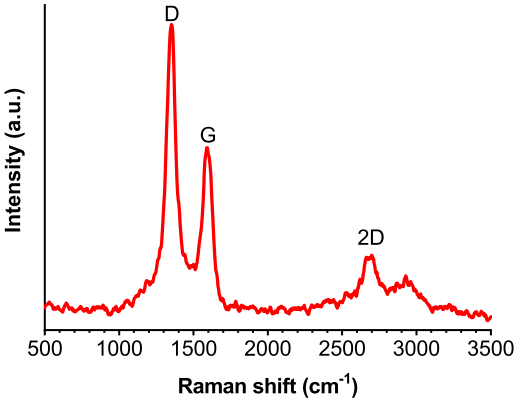

FIGURE 1. Raman spectra of the deposited NCG film.

TABLE 1. Raman spectra parameters.

Growth time (min)	I_D/I_G peak (intensity ratio)	FWHM (D) (cm^{-1})	FWHM (G) (cm^{-1})
35	2.34–2.39	70–72	64–78

The electrical conductivity of NCG thin films (σ_{NCG}) as a function of their thickness is presented in Fig. 2. At ∼250 nm, a relative saturation of the conductivity is observed, as the substrate's impact on the growing NCG decreases and the ion etching of amorphous carbon is likely to have a higher intensity, thus forming better conductive paths in the NCG as it grows on a sp^2 hybridized sublayer [21]. For higher values, an acceptable margin of error of ∼6% must be considered (corresponding to a maximum fluctuation of ±1000 S/m), also due to errors in the four-point probe electrical characterization.

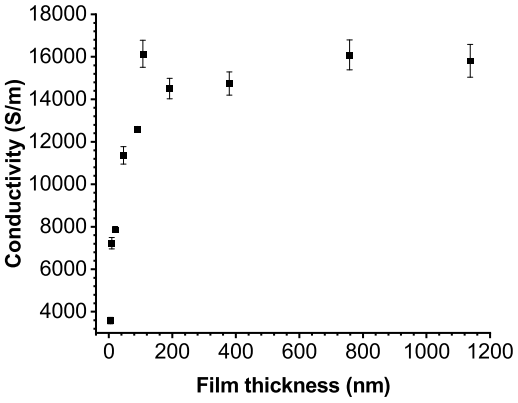

FIGURE 2. Electrical conductivity of NCG thin films as a function of their thickness.

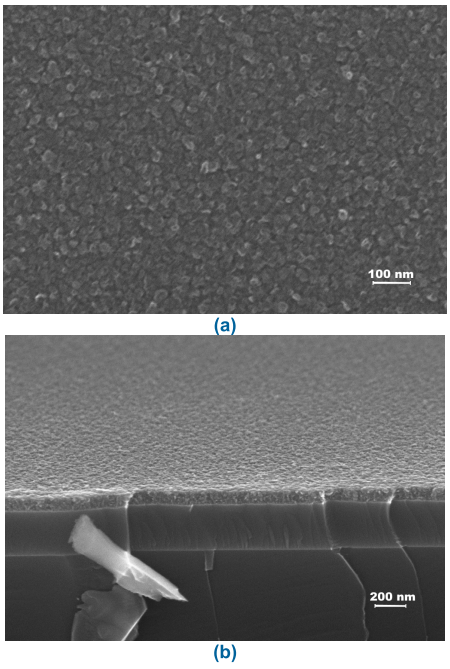

FIGURE 3. SEM images for (a) top-view and (b) cross-section of the fabricated NCG thin film.

Finally, two SEM pictures of the fabricated NCG layer are presented in Fig. 3. The images show a compact film with a columnar structure, the top view revealing nano-graphitic crystallites characteristic to this type of material [22].

Before starting the design of the NCG-based antenna array, the electrical performance of the fabricated NCG film was measured by using a four-point probe system. The on-wafer characterization was performed in the center of the 100-mm NCG wafer. No geometrical correction factor was applied, because the wafer area could be considered infinite and the NCG film was much thinner than the distance between the probes. The measured sheet resistance was 579 Ω/□, for the NCG film having the thickness of about 110 nm. The bulk resistivity was calculated to be 6.2 mΩ·cm, which is equivalent to a bulk conductivity of 16150 S/m (this value of the measured σ_{NCG} was then used to define the NCG layer

inside the EM simulator). Having this in mind, NCG films consist of nanocrystalline graphite domains immersed in a minimal amorphous phase. As such, they are an intermediate phase between crystalline and amorphous forms (with locally graphene-based fragments), and their basal-plane electronic conductance is higher than that along the perpendicular direction [23]. Moreover, the high crystallinity of the NCG (which comes from a negligible content of sp^3 carbon atoms) is one of the main reasons beneath the outstanding conductivity of such material. This conductivity can be tuned thanks to the carbon-like nature of the NCG, since the complex relative permittivity ε_r is a function $\mathscr{F}$ of the carrier density (electrons and holes) n_c and of the external applied voltage V_{ext}:

$$\varepsilon_r = \mathscr{F}(\alpha n_c V_{ext}) \tag{1}$$

where α is a geometrical constant. In other words, one can induces free carriers (either electrons in the conduction band with a positive V_{ext}, or holes in the valence band with a negative V_{ext}), thus changing the permittivity of the NCG material or, equivalently, its conductivity, since $\varepsilon_r = \varepsilon' - j\varepsilon''$ and $\varepsilon'' = \sigma_{NCG}/(\omega\varepsilon_0)$, with σ_{NCG} the complex conductivity (real in the microwave range), ω the angular frequency and ε_0 the vacuum permittivity. This fact can be explained by the interconnection between ε' and ε'' by the Kramers-Kronig relations, which relate the real and imaginary parts of the complex refractive index and, as a natural extension, it applies to the complex relative permittivity. However, in the case of the NCG, n_c and V_{ext} have a predominant effect upon ε'' or, in other words, on the bulk conductivity of this carbon-like material. Besides this, NCG exhibits an asymmetric Dirac-like peak of its resistance R_{NCG} (hence, conductance $G_{NCG} = 1/R_{NCG}$) at room temperature [20], with the charge type changing from electron to hole, depending on V_{ext}. This unique physical behavior is the key to understand the novelty of this work, in which the intrinsic properties of a material are used to confer tunability characteristics to an antenna array, without the need of using complex geometries and/or biasing techniques.

For the specific NCG under study, we can express σ_{NCG} as follows:

$$\sigma_{NCG} \approx N_{layer}\sigma_G \tag{2}$$

$$\sigma_G = \mathscr{G}(\omega, \mu_c) \tag{3}$$

$$\mu_C = \hbar v_F \sqrt{\pi \alpha_0 |V_{ext} - V_D|} \tag{4}$$

where σ_G is the surface conductivity of monolayer graphene, which is a function $\mathscr{G}$ of ω and of the chemical potential μ_c ($\mathscr{G}$ can be obtained by manipulating the well-known Kubo formula), N_{layer} is the number of graphene monolayers, $\hbar$ is the reduced Planck's constant, $v_F = s_F \times 10^6$ m/s is the Fermi velocity and $0 < s_F \leq 1$ is a scale factor, $\alpha_0 = 9 \times 10^6$ $m^{-2}V^{-1}$ is the fine structure constant, and V_D is the Dirac voltage. Typical values of μ_c fall within the range 0–1 eV. In other words, σ_{NCG} can be approximated reasonably with the conductivity of 320 graphene monolayers in parallel, which give rise to a crystalline graphite-like material.

Fig. 4 shows the calculated values of σ_{NCG} in the frequency range 0–30 GHz, at five values of μ_c: 0.15 eV, 0.25 eV, 0.5 eV, 0.75 eV, and 1 eV. It is evident how σ_{NCG} increases for increasing values of μ_c. One can observe that the measured σ_{NCG} fits very well with the calculated data if we consider a chemical potential $\mu_c = 0.15$ eV; this value corresponds to the application of a dc voltage of about 1.3 V when using the four-point probe system, which requires a small current (10 mA) passing through the two outer probes to induce a voltage between the two inner probes.

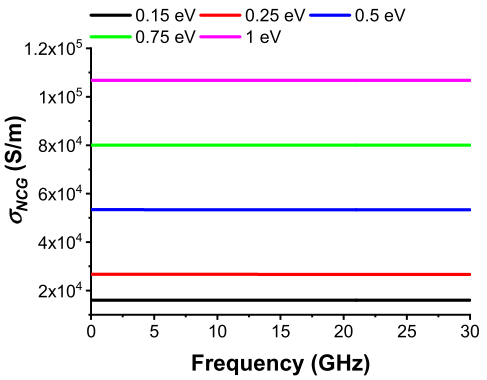

FIGURE 4. Calculated bulk conductivity of the 110-nm-thick NCG layer as a function of the chemical potential.

III. EM DESIGN AND SIMULATIONS OF THE NCG-BASED SINGLE PATCH AND 8-ELEMENT LINEAR ARRAY

The design of the NCG coplanar patch antenna (NCG-CPA) array started from the single NCG-based patch. The single NCG patch antenna was designed in CPW technology, since it is the easiest way to bias the NCG layer by applying an in-plane dc voltage between the central (or signal) line of the CPW and the lateral ground planes (as done in [15], but with the important difference that here we consider a patch antenna made of graphite directly grown on SiO_2, instead of monolayer graphene grown on a ferroelectric thin film). The layout of the single NCG-CPA in shown in Fig. 5, together with the main dimensions and a cross-section in the inset. The latter comprises a 525-μm-thick HRSi substrate, on top

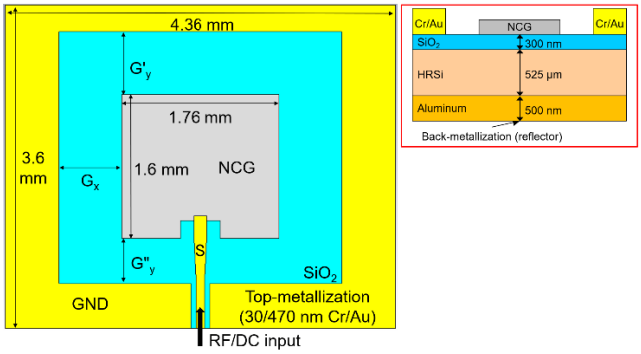

FIGURE 5. Top-view of the final NCG-CPA with the NCG layer as radiating element. Inset: cross-section of the antenna.

of which a 300-nm-thick SiO_2 layer is grown (in view of the NCG deposition). The metallization is a 500-nm-thick aluminum (Al) reflector on the back of the HRSi substrate, and a chrome/gold (Cr/Au) layer on top of the SiO_2 film for the CPW contacts.

In Fig. 5, $G_x = G'_y = 0.7$ mm, $G''_y = 0.5$ mm and the CPW port has gap-signal-gap dimensions of 60-100-60 μm (this is necessary for on-wafer measurements using standard CPW probe tips with pitch of 150 μm and ensures a characteristic impedance of 50 Ω on silicon substrate). G_x, G'_y and G''_y are the gaps between the patch and the ground plane; these distances were optimized to ensure the correct operation of both the antenna and the final array in terms of both reflection coefficient $|S_{11}|$ at the input port and radiation performance, guaranteeing at the same time an easy polarization of the NCG patch when applying an in-plane bias between the signal line S and the ground plane GND. The EM simulations were carried out using the 3D EM tool CST Microwave Studio®, the results being shown in Figs. 6a-c for both gold and NCG single patch with the same dimensions (the gold patch having the same thickness of 110 nm as the NCG patch for a correct comparison). With respect to the NCG-CPA, from Fig. 6a one can notice that $|S_{11}| < -6$ dB all over the 24-GHz ISM band (24–24.25 GHz, which is a widely exploited frequency range for wireless applications), whereas from Fig. 6b it is apparent that the antenna has a series resonance in the reference band, with a real part close to 50 Ω for optimal impedance matching to the CPW port. Also, Fig. 6c demonstrates that, as expected, the radiation of the patch is broadside (H-plane, solid black line), with a small tilt at $\phi = 20°$ (E-plane, solid red line), a maximum radiation efficiency of about 31% and a maximum gain of 0.29 dBi. The latter performance indicators are noteworthy, since conventional graphene-based antennas at microwaves exhibit a low radiation efficiency due to the high surface resistance, making them unfeasible for practical telecommunications systems. For this reason, graphene-based inks, multilayer graphene, or highly conductive graphene films are preferred to achieve radiation performance comparable to those of metal antennas. Moreover, such solutions are often neither reproducible nor suitable for large-scale production. A comprehensive comparison with the actual state-of-the-art is provided in Table 3 at the end of Section V.

When considering the gold patch, the minimum of $|S_{11}|$ ($|S_{11}|_{min}$) shifts of 480 MHz towards higher frequencies (hence, the gold antenna should be enlarged to resonate at the same frequency as the NCG one) and with worse matching properties, since $|S_{11}|_{min} = -10.16$ dB (in the case of the NCG-CPA $|S_{11}|_{min} = -16.39$ dB). From the radiation point of view, the maximum gain at 24 GHz is 3.45 dBi and the maximum radiation efficiency is about 65%. However, if we take the total efficiency η_{TOT} at 24 GHz into account, i.e., the ratio of the radiated power to the stimulated power of the antenna, the gold patch has $\eta_{TOT} \approx 32\%$, whereas the NCG patch has $\eta_{TOT} \approx 25\%$, thanks to the fact that the matching of the NCG-CPA is better than that of the Au-CPA.

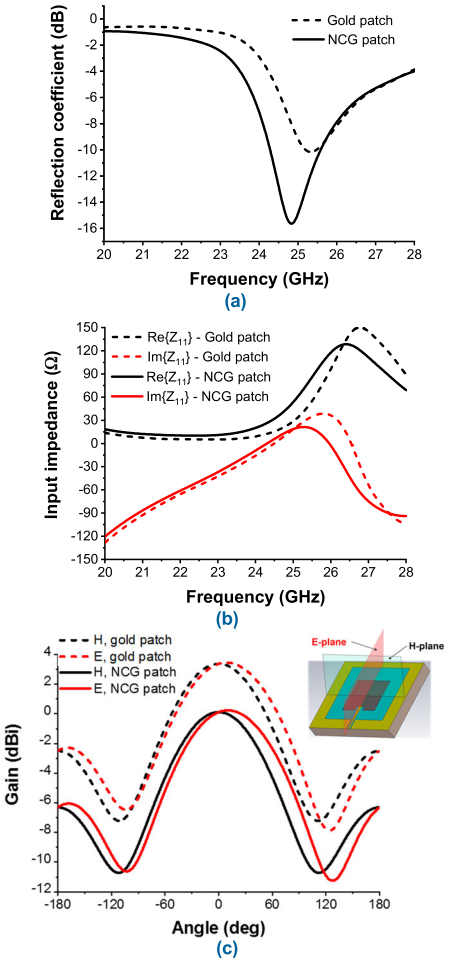

FIGURE 6. Simulated (a) reflection coefficient $|S_{11}|$ (dB), (b) input impedance Z_{11} (Ω) (black lines: real part; red lines: imaginary part), and (c) gain at 24 GHz (black lines: H-plane; red lines: E-plane; inset: visual explanation of H- and E-plane) of the single NCG-CPA and Au-CPA.

In Fig. 7, we show how the gain $G_{NCG-CPA}$ (in the H-plane) of the single NCG-based patch antenna changes when the conductivity of the NCG layer spans between 4000 S/m and 28000 S/m (hence, a variation of ±75% around the nominal value of 16000 S/m). This range is an estimation done after preliminary experiments carried out to quantify the change in the conductivity of the NCG when applying a V_{ext} of ±25 V (the minimum/maximum V_{ext} used for the dc/RF characterization).

One can notice that $G_{NCG-CPA}$ varies between -1.62 dBi and 0.85 dBi, whereas the resonance frequency undergoes a shift of 130 MHz. However, when designing the 8-element linear array, the total gain G_{array} can be defined as follows:

$$G_{array} = \beta N G_{NCG-CPA} \tag{5}$$

where $0 < \beta < 1$ is a correction factor that considers the spacing between adjacent elements, EM couplings, the presence of the feeding network, technological uncertainties and, finally, the non-ideality of the array. $N = 8$ is the number of array elements. We stress here that the impact of the inter-element spacing is quite significant, as it was also

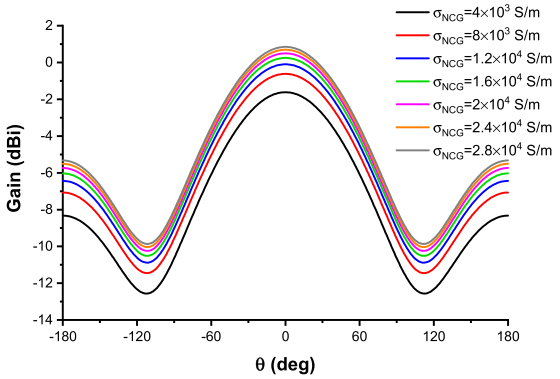

FIGURE 7. Simulated gain (dBi) of the single NCG-CPA at 24 GHz in the H-plane, as a function of NCG film's conductivity.

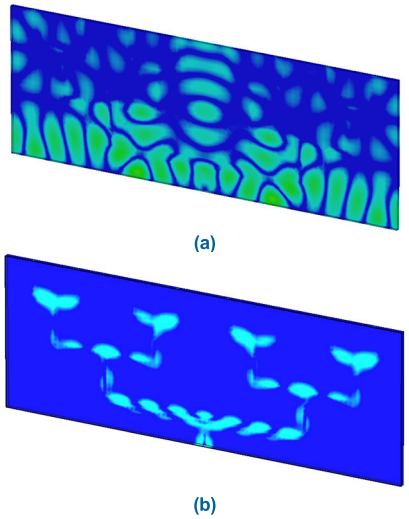

FIGURE 8. Simulated electric-field distribution of the corporate feed network (a) with back reflector and (b) without back reflector.

demonstrated in [24]. In particular, the optimal spacing for beam forming or MIMO applications [25] could be not necessarily $\lambda_0/2$ (which was our choice in the present work, due to design and technological constraints, i.e., the exploitation of non-conventional materials for the radiators and the available occupation area of the array – just 4×3 cm^2 – to be integrated into a transmit/receive module together with other devices/components). The next step was the design of the entire 8-element NCG-CPA array. First, the basic CPW T-junction was designed, as follows: for a balanced phase and amplitude distribution among the eight radiators, the distance between the outputs is set to 4.36 mm. Input and outputs impedances are equal to 50 Ω, whereas two 70-Ω quarter-wavelength stubs are used to match the input and the outputs. Optional bonding wires can be positioned on the discontinuities (junction and bends) to further guarantee the continuity of the ground plane along the structure. Once the T-junction was optimized at 24 GHz, it was cascaded to build an 8×1 linear network. At this stage, from EM simulations we observed that the performance of the network was poor in terms of both efficiency and amplitude stability of the output signals. A possible explanation for the simulated performance degradation was the generation of surface waves triggered by the back Al reflector plane (Fig. 8a) that was kept from the design of the single NCG-CPA (inset of Fig. 6c). Once the reflector plane was removed under the corporate feed network (and kept only beneath the NCG-based patches), the electric field is better guided by the structure, which significantly improves the performance (Fig. 8b). Finally, the corporate feed network was integrated with the 8 NCG-CPAs and simulated.

The reflection coefficient and the radiating performance are shown in Fig. 9a and Figs. 9b-c, respectively. In these figures, the results obtained for the array in two configurations are presented: with a plexiglass slab (with a thickness of 9 mm) under the HRSi substrate and without it. The plexiglass slab has a conformal shape (inset of Fig. 9a), in the sense that it follows solely the external perimeter of the array. The motivation for such a design solution is twofold: (i) necessity of using a low-κ dielectric support for both on-wafer and far-field measurements, as to avoid the usage of a metal plate in direct contact with the silicon (thus eliminating the surface waves mentioned before); (ii) further simulations revealed that the presence of the plexiglass under both the NCG-CPAs and the corporate feed network could affect in a destructive way the radiation properties with respect to the case of the array in free space. Furthermore, in the final prototype a ROHACELL® HF layer was used to fill the space under the array where no plexiglass was present (to increase the mechanical robustness), this foam material being the ideal choice for microwave applications due to its permittivity close to 1 and its low dielectric loss tangent. As it can be seen from Figs. 9a-c, the reflection coefficient and the gain at 24 GHz (in both the H- and E-plane) are not affected dramatically by the foreseen support structure (conformal plexiglass and ROHACELL) exploited to ensure reliable high-frequency characterization. In particular, the maximum value of G_{array} with the plexiglass slab is 3.22 dBi in the H-plane (at $\theta = 0°$) and 5.36 dBi in the E-plane (at $\phi = 51°$): this demonstrates the importance of simulating rigorously the effective structure that will be deployed for measurements, to consider any EM effects due to the complete assembly.

These simulations gave us useful information for the subsequent interpretation of the measurements. In a real wireless application, the array is integrated directly on chip into a front-end, and the design of the impedance dividers is carried out taking into consideration the complete vertical structure of the underneath substrate. In the inset of Fig. 9a one can notice a CPW section meant for the integration of the NCG-CPA array with the SMPM connector for far-field measurements in free space. The input port is normalized on 50 Ω and can fit CPW probe tips with a pitch of 500 μm as well. Fig. 9 also demonstrates that, if using an array entirely made of gold patch antennas (with a metal thickness that is equal to the thickness of the NCG layer), the obtained performance is just slightly better (due to evident skin depth effects that jeopardize the advantage of having a high conductivity),

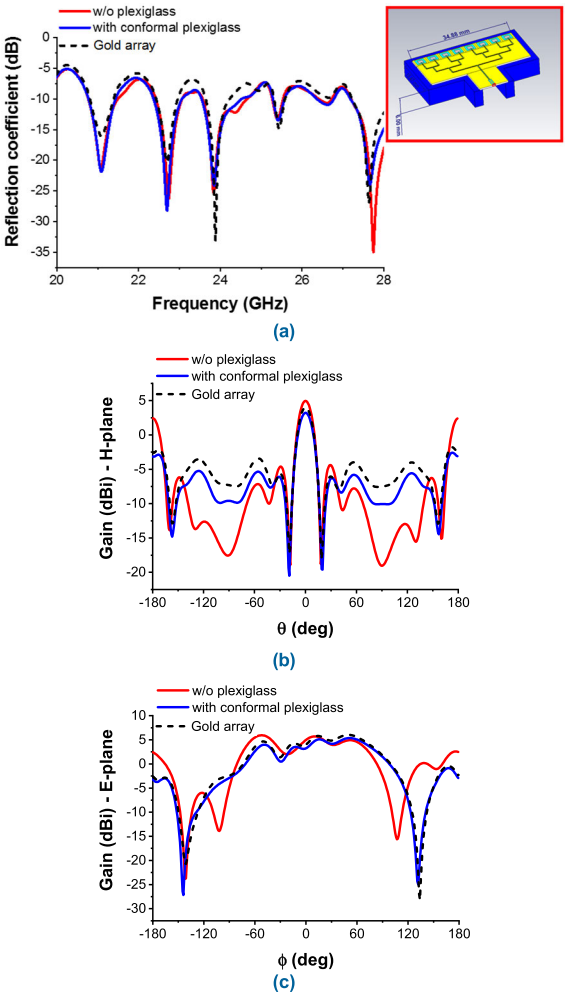

FIGURE 9. Simulated (a) reflection coefficient $|S_{11}|$ (dB) (inset: simulated 3D structure) and gain for the (b) H-plane and (c) E-plane of the NCG-CPA array at 24 GHz, without (solid red line) and with (solid blue line) the conformal plexiglass slab, and of the Au-CPA-array (dashed black lines).

but at the cost of not having the possibility of tuning the array gain. Table 2 summarizes the main performance indicators for the two case of gold patch antennas and NCG patch antennas used in both single and array configuration. It is apparent how, especially for the array, the proposed solution with NCG-CPAs is more exploitable thanks to the intrinsic tunability of the carbon-based material.

IV. FABRICATION OF THE NCG-BASED 8-ELEMENT LINEAR ARRAY

The proposed workflow for the fabrication process of the 24-GHz NCG-CPA arrays is as follows: wafer cleaning, thermal oxidation, NCG deposition, photolithography for NCG patterning, NCG etching, photolithography for metal patterning, Cr/Au deposition, lift-off, Al backside metallization, photolithography for backside metal patterning, and Al etching. To test the proposed workflow, n-type Si wafers were used, 100 mm diameter, <100> orientation (Miller index, which indicates the orientation of a plane or set of parallel planes of atoms in the silicon crystal), 525+/-25 μm

TABLE 2. Simulated performance for gold and patch antennas.

Type of antenna	Directivity @ 24 GHz (dBi)	Gain @ 24 GHz (dBi)	Radiation efficiency (%)	Total efficiency (%)
Gold patch	5.29	3.45	65	32
NCG patch	5.39	0.29	31	25
Gold array	8.25	4	38	37
NCG array	8.31	3.22	31	30

thickness, and resistivity 1–10 Ω·cm. Before any processing, the Si wafers were cleaned in acetone, isopropyl alcohol, and Piranha solutions. The same procedure was performed before spin coating for each photoresist mask.

After the proposed workflow was successful, for the final device fabrication a 4-inch wafer of 525-μm-thick HRSi was used (Float-Zone Hyper Pure Silicon (FZ-HPS) P(100) by Topsil, resistivity $\rho > 10,000$ Ω·cm). Wafer cleaning procedure: (i) initial soak in acetone for at least 10 min; (ii) rinsing in isopropyl alcohol (IPA) for at least 10 min; (iii) immersion in Piranha solution (H_2SO_4+H_2O_2, 10:1) at 120°C for 30 min; (iv) rinsing with deionized water. The thermal oxidation was performed in the Thermco 2000 series (Tetron Technologies, UK) oxidation furnace. The thermal oxide was grown in wet atmosphere at 1100°C in the oxidation furnace. The final thickness of the thermal oxide was ∼300 nm.

The NCG deposition was performed as described above. The metal deposition was done in the Auto 500 (BOC Edwards, UK) electron beam deposition system. The total thickness of the Cr/Au metal layer deposited on the front side of the wafer was 500 nm (30 nm Cr and 470 nm Au), whereas the thickness of the backside Al was 500 nm. Photolithography was performed using the MA6 (MicroSüss, Germany) mask alignment system. As masking layer, a HPR 504 positive photoresist was used. The etching of the NCG thin film was done in the SI220 (Sentech Instruments, Germany) reactive ion etching system, in an O_2 plasma using the chemical etching mode at 250 W and 150 mTorr. The NCG thin film was etched using the process described earlier, the etch rate was approximately 50 nm/min, resulting in a total etch time of about 2 min. The complete removal of the NCG in the unwanted areas (other than those corresponding to the patch antennas) was determined by four-point probe electrical measurements.

The Cr/Au metal layer deposited on the front side of the wafer was patterned using a lift-off process. First, a HPR 504 photoresist was spin coated on the front side and patterned using the corresponding photolithographic mask, followed by metallization. The photoresist was then removed using acetone in an ultra-sound bath. After cleaning the wafer in acetone and IPA, the HPR 504 photoresist was spin coated on the front side of the wafer to act as a protective layer during backside processing. A layer of Al, 500 nm thickness, was deposited on the backside of the wafer. The HPR 504 was patterned with the corresponding etching mask. The Al layer was etched in a solution of H_3PO_4+HNO_3+CH_3COOH+H_2O (ratio 8:5:5:10).

Six NCG-CPA arrays were fabricated on a single 4-inch HRSi wafer, as the one shown in Fig. 10. The array has total dimensions of 34.88 mm × 25.47 mm.

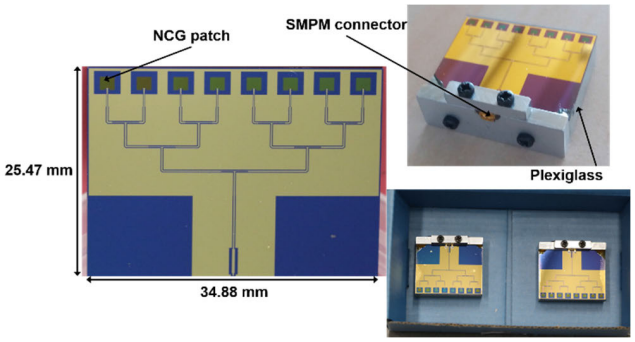

FIGURE 10. Fabricated array (left), array mounted on plexiglass and bonded to the SMPM connector (upper right; a metal support was also attached to the array and the plexiglass to guarantee the electrical connection with the connector), and prototypes ready to be sent for far-field characterization (lower right).

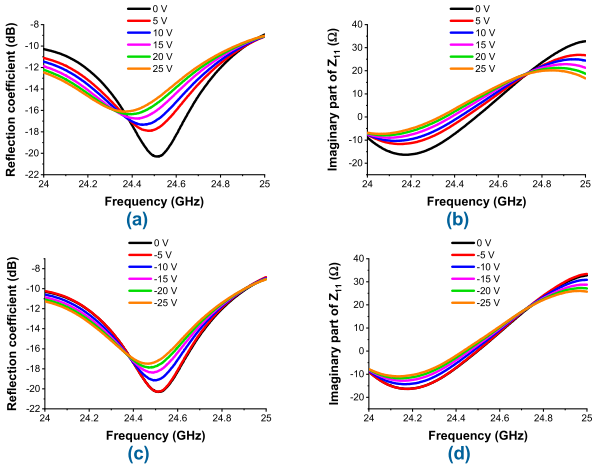

FIGURE 11. Measured (a) reflection coefficient and (b) imaginary part of array's input impedance for positive DC bias; measured (c) reflection coefficient and (d) imaginary part of array's input impedance for negative DC bias. In Figs. 11c-d, the solid red curves (corresponding to -5 V) are very close to the solid black ones (corresponding to 0 V).

V. EXPERIMENTAL CHARACTERIZATION OF THE 24-GHz NCG-BASED 8-ELEMENT LINEAR ARRAY

The measurements of the NCG-CPA array were carried out as follows: first, the on-wafer scattering parameters (Fig. 11) were measured with a calibrated (Short-Open-Load) vector network analyzer (VNA, Anritsu 37397D), by using special probe tips with a pitch of 500 μm. Connecting the NCG-CPA array to a dc source via a bias tee, it was possible to demonstrate the bias-dependent behavior of the array's reflection coefficient. More in detail, positive and negative dc bias voltages were applied, which put in evidence the asymmetry of the 110-nm-thick NCG layer as regards the tunability of its conductivity.

From Figs. 11a-d one can observe that in the band 24–25 GHz, for positive dc bias voltage values (Fig. 11a) there is a frequency shift of 158 MHz in the $|S_{11}|$ minimum, which is associated to a change of more than 4 dB in terms of matching properties; this means a difference of 2.5× times in the power reflected by the array. The same can be seen in the imaginary part of the input impedance $\mathrm{Im}\{Z_{11}\}$ (Fig. 11b). In this case, the resonance frequency shifts from 24.498 GHz down to 24.332 GHz (i.e., a resonance shift of 166 MHz). When switching to negative dc bias voltage values, the $|S_{11}|$ minimum (Fig. 11c) down-shifts of 50 MHz, with a change of about 2.8 dB or, in other words, a difference of about 2× times in the power reflected by the array. As regards $\mathrm{Im}\{Z_{11}\}$ (Fig. 11d), for a negative bias the resonance frequency shifts from 24.498 GHz down to 24.432 GHz (i.e., a resonance shift of 66 MHz). Hence, it can be concluded that the tuning effect (in both magnitude of $|S_{11}|$ and resonance frequency) is evident for both positive and negative dc bias voltages, but more pronounced for the former. This means that the 110-nm-thick NCG layer experiences a change of its microwave conductivity, which translates into (i) different matching behavior to 50 Ω and (ii) different resonance frequency in the band 24–25 GHz.

For the microwave characterization of the NCG-CPA array, two different customized measurement systems were prepared. First, the far-field characterization was performed (Fig. 12) with an array prototype connected to an SMPM connector, by using the experimental setup described in Appendix A.

In Figs. 12a-b, the simulated and measured gain values in the H-plane are presented (for the case of unbiased NCG), the latter as it was calculated using the far-field measurements around 24 GHz (the shape of the radiation pattern being similar in the band of interest). In Fig. 12a the solid red curve refers to the measured co-polarization gain G_{co-pol}, whereas the dotted black curve identifies the simulated G_{co-pol}; in Fig. 12b, the solid red curve and the dotted black curve represent the measured and simulated cross-polarization gain $G_{cross-pol}$, respectively. In other words, the linear polarizations of the NCG array and of the reference horn antenna are either parallel (co-polarization, maximum transmission between transmitter and receiver) or perpendicular (cross-polarization, minimum transmission between transmitter and receiver). These measurements are important, in the sense that they provide the clear proof of the effective radiative behavior of the NCG array, which entails a $|G_{co-pol} - G_{cross-pol}|$ of several dB; in the present case, $|G_{co-pol} - G_{cross-pol}| \approx 20$ dB in the broadside direction ($\theta = 0°$).

From the gain patterns, it results that the antenna radiates broadside in the H-plane and the maximum measured gain is 2.6 dBi around 24 GHz, whereas the simulated one is about 3.2 dBi, with a good agreement between simulations and experiments despite the unavoidable differences, as evidenced by the positions of the minima. The latter fact could be ascribed to the following main reasons: (i) the correction factor β (even if in this case the antenna spacing is given), which appoints technological uncertainties (like the margin of error of ∼6% in NCG's conductivity or corrosion-related defects)

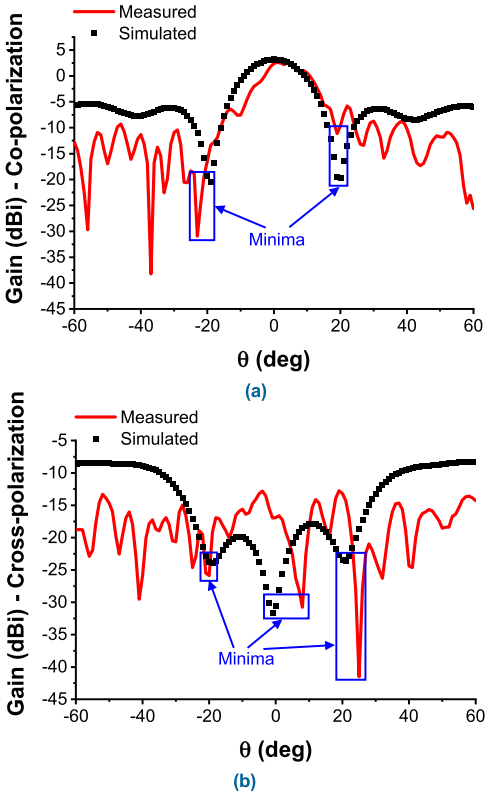

FIGURE 12. Measured (solid red curves) and simulated (dotted black curves) gain in the H-plane for both (a) co-polarization and (b) cross-polarization in the angular range $\theta \in [-60°, 60°]$, for the case of unbiased NCG.

as the main cause for the observed discrepancies; (ii) the lack of the SMPM connector and of the fabricated metal support in the EM simulations for ease-of-computation; (iii) the far-field standard open-space characterization setup, which could explain the fluctuations of the gain for values below −10 dBi. Nevertheless, the measured half-power beam width (HF-BW) is 14.5° (hence, smaller than the simulated value equal to ∼18°), and the measured $|G_{co-pol} - G_{cross-pol}|$ in the HF-BW is between 13 dB and 31.8 dB. This means that the HF-BW (the $|G_{co-pol} - G_{cross-pol}|$ difference) is narrow (big) enough to guarantee a good radiation performance with satisfactory gain values in the desired polarization plane, suitable in wireless links where a high directivity is envisaged (especially considering the conductivity of the NCG film, which is 3 orders of magnitude lower than gold).

Second, the accurate voltage-controllable tunability of the NCG film for modulation of array's transmission (or reception) properties was demonstrated. For this purpose, another measurement setup was prepared (as explained in Appendix B) to ensure a precision of just a few fractions of dB. In Fig. 13 the measured results for the gain of the NCG-based array (H-plane, co-polarization) are displayed at three frequencies of interest in the 24-GHz ISM band, namely at 24 GHz, 24.12 GHz, and 24.25 GHz, as a function of the applied dc bias voltage.

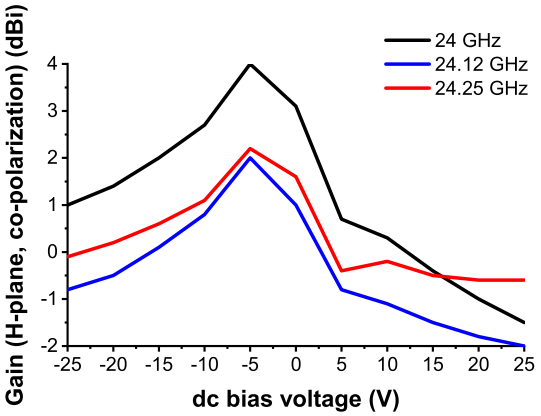

FIGURE 13. Measured gain (H-plane, co-polarization) of the NCG-based array, at three frequencies of interest in the 24-GHz ISM band (solid black line: 24 GHz; solid blue line: 24.12 GHz; solid red line: 24.25 GHz), as a function of the applied dc bias.

The curves in Fig. 13 give the final proof of the tunability potential offered by the proposed NCG-CPA array: when spanning the bias between -25 V and 25 V, the voltage applied in-plane onto the NCG layer allows changing the gain with 2.8 dB (at 24.25 GHz) up to 5.5 dB (at 24 GHz), with a maximum at -5 V and a minimum at 25 V for all the three considered frequencies. Since the gain can be tuned with 5.5 dB at 24 GHz and considering that, around the same frequency, the maximum value of the measured G_{array} is ∼3 dBi in the unbiased case (in the H-plane and in the co-polarization case, as extracted by the measurements of the power received by the horn antenna performed with the setup described in Appendix B), G_{array} can be tuned continuously at 24 GHz between 4 dBi and −1.5 dBi. This is a remarkable result, considering that such radiation performance related to an NCG-based array has not been yet reported. Due to the intrinsic nature of the NCG layer, the biasing effect is asymmetric around 0 V. More in detail, as explained in Section II, the NCG exhibits an asymmetric Dirac-like peak of its resistance at room temperature [20], i.e., the conduction mechanism due to electrons differs from the one due to holes. A particularly important aspect is that the tuning effect is instantaneous, meaning that the conductivity value of the NCG film can be changed very fast, without any latency phenomenon, thus offering a real-time reconfigurability of the array. Finally, the optimized PECVD process allowed obtaining a high fabrication yield, thanks to an optimal homogeneity of the NCG thin film: a single HRSi/SiO_2 4-in wafer can embed up to six arrays (as already stated), all of them exhibiting almost constant performance, with a margin of error of just 2-3%.

Now we present a possible application of practical interest of the proposed NCG-based array, namely an indoor localization system based on a 24-GHz ISM band frequency-modulated continuous-wave (FM-CW) radar that embeds small, codified tags for identification functionality [15]. In this case, the maximum transmitting distance d is between 50 and 70 m. The transmitting antennas do not

require any specific gain because of regulation constraints for the maximum effective isotropic radiated power (EIRP), i.e., $EIRP_{max} = 20$ dBm; as regards the receiving antennas, gain values in the range 15–20 dBi are generally targeted to maximize the communication distance. Last, the isolation between transmitting and receiving antennas should be at least 30–40 dB. If the proposed NCG-based array is used, it is straightforward to calculate realistic values of the power P_r received by the array as a function of both distance d and applied dc bias. The results are shown in Fig. 14 for $EIRP_{max} = 20$ dBm.

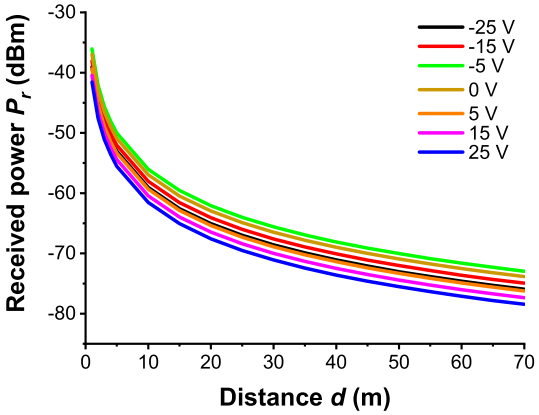

FIGURE 14. Calculated power P_r received by the proposed NCG-based array in a FM-CW radar application, as a function of both distance d and applied dc bias.

One can see from Fig. 14 that, spanning the dc bias voltage between −25 V and 25 V, P_r increases of 5.5 dB from 25 V (worst case) to −5 V (best case), thus following the behavior of antenna gain (as expected). For example, at 1 m distance $P_r = -41.5$ dBm at 25 V and $P_r = -36$ dBm at −5 V, whereas at 70 m distance $P_r = -78.5$ dBm at 25 V and $P_r = -73$ dBm at −5 V. Considering a realistic value of −100 dBm for a typical 24-GHz receiver sensitivity, this entails that the attenuation margin is always in the range 21.5–64 dB, i.e., it is big enough to guarantee a low bit error rate (BER). More than that, the real-time amplitude modulation of the gain allows a fine tuning of the power received at a targeted distance by simply changing the dc bias applied to the NCG film. This simple theoretical example (based on a realistic scenario) gives a proof of the potential offered by NCG materials for modern (and future) telecommunications systems.

Finally, Table 3 presents a comparison between the proposed NCG-based array and some of the latest works in the literature regarding graphene antennas in microwaves. In this table, ''Type'' is the type of graphene-like material, f is the operating frequency (or band), G_{max} is the maximum gain, η_{max} is the maximum efficiency, ''sim.'' or ''meas.'' indicates that the reported result is simulated or measured, and ''Tune'' refers to the tunability characteristics of the antenna.

As a further proof of what has been already demonstrated in the literature (i.e., the fact that microwave applications of graphene for radiators are avoided due to high losses), [26]–[28] report only simulated results for both G_{max} and η_{max}, with [27] and [28] using too optimistic values of R_s in biased state. Besides this, even if [28] exploits graphene monolayer's tunability to modulate the gain (the graphene being used for the directors, nor for the driven element), it does not show how it could be realized from a technological point of view: it is declared that the silicon sheet acts as the ground plane for the polarization, but this would be possible only if it were a low-resistivity silicon layer, which hinders any antenna application at microwaves. Last, in [30]–[32] the authors show measured results with high gain and efficiency values but losing completely the tunability of graphene at the expense of highly conductive graphene-based films (in [32], the nanoplates are used to load a power dividing feed line to manipulate the phase of the radiation pattern, whereas the multilayer graphene film MGF is used to fabricate metal-like radiators). From this brief comparison, we can state that the solution proposed in this work could overcome the bottleneck ''high conductivity vs. tunability'' of carbon-based antennas, offering interesting new perspectives and solving the problem that the authors in [33] raised about the feasibility of graphene for microwave applications.

TABLE 3. Comparison between the proposed NCG-based array and the state-of-the-art graphene antennas at microwaves.

Ref.	Type	σ or R_s	f (GHz)	G_{max} (dBi)	η_{max} (%)	*Tune*
[26]	Ink	2.5×10^4 S/m	3–6	3.15 @6GHz Sim.	88 @3GHz Sim.	No
[27]	Multi -layer	25 Ω/□	3.5–9.5	5.36 @9.5GHz Sim.	83.2 @3.5GHz Sim.	No
[28]	Mono -layer	6–2580 Ω/□	5.5	10.74 Sim.	89.7 Sim.	Yes
[29]	LrGO	50–200 Ω/□	0.847	–	–	–
[30]	High-σ film	1×10^6 S/m	2.45–5.2	6.29 @5.2GHz Meas.	86.3 @5.2GHz Meas.	No
[31]	High-σ film	~1×10^6 S/m	5–6.4	6 @5.6GHz Meas.	90 @5.6GHz Sim.	No
[32]	Nano-plates and MGF	20–210 Ω/□ (nano-plates)	30	15.5 Meas.	65	Yes (nano-plates)
This work	NCG	1.6×10^4 S/m	24-GHz ISM band	~4 @-5V dc bias Meas.	~30 Meas.	Yes

VI. CONCLUSION

In this manuscript, we have presented a 110-nm-thick nanocrystalline graphite (NCG) film, grown by plasma enhanced chemical vapor deposition and used to fabricate the radiating elements of a 24-GHz patch antenna array. The NCG exhibits an exceptional bulk conductivity exceeding 16000 S/m, thus several orders of magnitude higher than that of graphene monolayers. However, the NCG keeps the unique signature of mono- and multi-layer graphene, i.e., the modulation of its charge carrier density (or, in other words, its electrical conductivity) by applying an external static electric

field. As a result, we succeeded in tuning both the resonance frequency (with 166 MHz) and gain (with 5.5 dB) of the fabricated NCG-based array when biasing in-plane the NCG film between −25 V and 25 V. This result is particularly important, as it demonstrates how a 3D carbon-based material like NCG can be profitably used to create new CMOS-compatible microwave components with reconfigurability characteristics based solely on the intrinsic characteristics of the constitutive materials, not requiring any complex polarization network and with the potential of large-scale (hence, cost-effective) production. The presented outcomes could serve as a promising starting point for further research in this field.

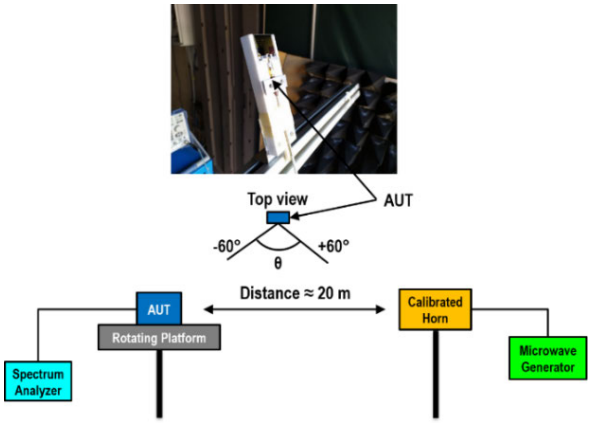

FIGURE 15. Far-field measurement setup.

APPENDIX

A. FAR-FIELD MEASUREMENTS

The antenna under test (AUT in Fig. 15) was mounted on a rotating platform (with a precision of 0.25°) to allow for the measurements on the azimuth (θ) plane from −60° to 60°, in a standard open-space characterization setup. Once mounted, the connectorized AUT (receiver) was connected to a spectrum analyzer (Rohde & Schwarz FSV40-N). Then, a calibrated horn with gain of 17.7 dBi (transmitter), placed at 20 m from the AUT, was connected to a signal generator (Agilent E8257D) with an output power level of 14 dBm. A picture of the setup is displayed in Fig. 15.

We stress here that this setup is the same used to measure and validate Satcom antennas that work in the same frequency band as the proposed NCG-based array. The horn antenna is positioned at a height of about 8 m from the ground; therefore, the negative contribution of the soil is minimized (considering that the beam width of our antenna is less than 15°). From extensive measurements carried out to validate commercial Satcom antennas, it has been empirically proven that the gain accuracy is about 1 dB.

B. NCG FILM'S TUNABILITY MEASUREMENTS

To accurately verify the tunability of the NCG film under the application of a proper dc bias voltage, an array prototype (used as a transmitter) was connected to a microwave generator (Agilent E8257D) and to a dc source (Agilent E3631A)

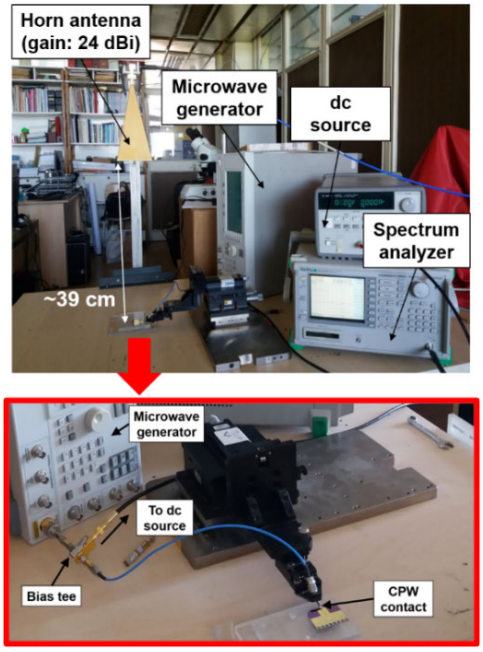

FIGURE 16. Microwave setup to characterize the NCG-CPA array. As mentioned in the text, a conformal plexiglass support was deployed to avoid destructive interferences related to the corporate feed network for proper power splitting. Red inset: detailed view of the excitation technique used for on-wafer measurements, with the bias tee and CPW contact in evidence.

directly on-wafer (i.e., without the SMPM connector), using CPW probe tips and a bias tee (a comprehensive picture of the setup is displayed in Fig. 16). This way, it was possible to change the frequency, the input power, and the dc bias level of the array. The receiver was a high-gain K-band horn antenna (with gain of 24 dBi) connected to a spectrum analyzer (Anritsu MS2668C), to measure the level of power transmitted by the array. The horn antenna was placed at ∼39 cm, which corresponds to ∼31 × λ_0 (where λ_0 is the free-space wavelength at 24 GHz). This ensured that the horn antenna was in the Fraunhofer region of the array.

We stress here that we also used microwave absorber panels (Cuming Microwave C-RAM FAC-1.5 24 × 24″ w/Velcro) around the two antennas (not shown in Fig. 16), to limit potential interferences and multi-path effects due to the surrounding equipment. The reliability of the used setup was verified by carrying out tens of measurements on different NCG-based arrays, which provided the same outputs (in terms of transmitted power) with a negligible margin of error.

ACKNOWLEDGMENT

The authors would like to thank Dr. Raluca Gavrila and Dr. Florin Comanescu from IMT-Bucharest for their assistance in NCG material's characterization.

REFERENCES

[1] M. Dragoman, D. Neculoiu, A.-C. Bunea, G. Deligeorgis, M. Aldrigo, D. Vasilache, A. Dinescu, G. Konstantinidis, D. Mencarelli, L. Pierantoni, and M. Modreanu, "A tunable microwave slot antenna based on graphene," *Appl. Phys. Lett.*, vol. 106, no. 15, Apr. 2015, Art. no. 153101.

[2] M. Dragoman, A. Cismaru, M. Aldrigo, A. Radoi, A. Dinescu, and D. Dragoman, "MoS_2 thin films as electrically tunable materials for microwave applications," *Appl. Phys. Lett.*, vol. 107, no. 24, Dec. 2015, Art. no. 243109.
[3] M. Dragoman, M. Aldrigo, J. Connolly, I. M. Povey, S. Iordanescu, A. Dinescu, D. Vasilache, and M. Modreanu, "MoS_2 radio: Detecting radio waves with a two-dimensional transition metal dichalcogenide semiconductor," *Nanotechnology*, vol. 31, no. 6, Jan. 2020, Art. no. 06LT01.
[4] A. Ahmed, I. A. Goldthorpe, and A. K. Khandani, "Electrically tunable materials for microwave applications," *Appl. Phys. Rev.*, vol. 2, no. 1, Mar. 2015, Art. no. 011302.
[5] T. Wang, W. Jiang, Y. Peng, and G. Wang, "Integration of ferromagnetic and ferroelectric films for fully electrically tunable RF devices," in *Proc. IEEE Radio Wireless Symp. (RWS)*, Jan. 2017, pp. 5–8, doi: 10.1109/RWS.2017.7885929.
[6] S. Pawar, J. Singh, and D. Kaur, "Magnetic field tunable ferromagnetic shape memory alloy-based piezo-resonator," *IEEE Electron Device Lett.*, vol. 41, no. 2, pp. 280–283, Feb. 2020.
[7] N. O. Weiss, H. Zhou, L. Liao, Y. Liu, S. Jiang, Y. Huang, and X. Duan, "Graphene: An emerging electronic material," *Adv. Mater.*, vol. 24, no. 43, pp. 5782–5825, Nov. 2012.
[8] C. Fan, B. Wu, R. Song, Y. Zhao, Y. Zhang, and D. He, "Electromagnetic shielding and multi-beam radiation with high conductivity multilayer graphene film," *Carbon*, vol. 155, pp. 506–513, Dec. 2019.
[9] X. Huang, T. Leng, M. Zhu, X. Zhang, J. Chen, K. Chang, M. Aqeeli, A. K. Geim, K. S. Novoselov, and Z. Hu, "Highly flexible and conductive printed graphene for wireless wearable communications applications," *Sci. Rep.*, vol. 5, no. 1, Nov. 2016,. Art. no. 18298.
[10] S. N. H. Sa'don, M. H. Jamaluddin, M. R. Kamarudin, F. Ahmad, Y. Yamada, K. Kamardin, and I. H. Idris, "Analysis of graphene antenna properties for 5G applications," *Sensors*, vol. 19, no. 22, p. 4835, Nov. 2019.
[11] A. Sarycheva, A. Polemi, Y. Liu, K. Dandekar, B. Anasori, and Y. Gogotsi, "2D titanium carbide (MXene) for wireless communication," *Sci. Adv.*, vol. 4, no. 9, Sep. 2018, Art. no. eaau0920.
[12] C. H. Ahn, A. Bhattacharya, M. Di Ventra, J. N. Eckstein, C. D. Frisbie, M. E. Gershenson, A. M. Goldman, I. H. Inoue, J. Mannhart, A. J. Millis, A. F. Morpurgo, D. Natelson, and J.-M. Triscone, "Electrostatic modification of novel materials," *Rev. Modern Phys.*, vol. 78, no. 4, pp. 1185–1212, Nov. 2006.
[13] A. K. Geim, "Nobel lecture: Random walk to graphene," *Rev. Modern Phys.*, vol. 83, no. 3, pp. 851–862, Aug. 2011.
[14] A. K. Geim, "Graphene prehistory," *Phys. Scripta*, vol. T146, Jan. 2012, Art. no. 014003.
[15] M. Aldrigo, M. Dragoman, S. Iordanescu, F. Nastase, D. Vasilache, and A. Ziaei, "Gain tunability of graphene patch antennas for the ISM band at 24 GHz," in *Proc. Int. Workshop Antenna Technol. (iWAT)*, Feb. 2020, pp. 1–4, doi: 10.1109/iWAT48004.2020.1570609136.
[16] M. E. Schmidt, C. Xu, M. Cooke, H. Mizuta, and H. M. H. Chong, "Metal-free plasma-enhanced chemical vapor deposition of large area nanocrystalline graphene," *Mater. Res. Exp.*, vol. 1, no. 2, May 2014, Art. no. 025031.
[17] A. Isacsson, A. W. Cummings, L. Colombo, L. Colombo, J. M. Kinaret, and S. Roche, "Scaling properties of polycrystalline graphene: A review," *2D Mater.*, vol. 4, no. 1, Dec. 2016, Art. no. 012002.
[18] O. Simionescu, R. C. Popa, A. Avram, and G. Dinescu, "Thin films of nanocrystalline graphene/graphite: An overview of synthesis and applications," *Plasma Processes Polym.*, vol. 17, no. 7, Jul. 2020, Art. no. 1900246.
[19] A. C. Ferrari and J. Robertson, "Interpretation of Raman spectra of disordered and amorphous carbon," *Phys. Rev. B, Condens. Matter*, vol. 61, no. 20, pp. 14095–14107, May 2000.
[20] S. K. Jerng, D. S. Yu, Y. S. Kim, J. Ryou, S. Hong, C. Kim, S. Yoon, D. K. Efetov, P. Kim, and S. H. Chun, "Nanocrystalline graphite growth on sapphire by carbon molecular beam epitaxy," *J. Phys. Chem. C*, vol. 115, no. 11, pp. 4491–4494, 2011.
[21] O.-G. Simionescu, E. Anghel, O. Tutunaru, C. Pachiu, R. Gavrila, A. Avram, O. Buiu, and G. Dinescu, "Correlation between the growth process and film properties of RF-PECVD grown nanocrystalline graphite/graphene," in *Proc. Springer Energy (SPE)*, 2020, pp. 399–410, doi: 10.1007/978-3-030-55757-7_27.
[22] S. J. Fishlock, D. Grech, J. W. McBride, H. M. H. Chong, and S. H. Pu, "Mechanical characterisation of nanocrystalline graphite using micromechanical structures," *Microelectron. Eng.*, vol. 159, pp. 184–189, Jun. 2016.
[23] D. Zhang, L. Peng, P. Yi, and X. Lai, "Electronic transport and corrosion mechanisms of graphite-like nanocrystalline carbon films used on metallic bipolar plates in proton-exchange membrane fuel cells," *ACS Appl. Mater. Interface*, vol. 13, no. 3, pp. 3825–3835, Jan. 2021.
[24] M. Aldrigo, D. Masotti, V. Rizzoli, and A. Costanzo, "Design rules for innovative nano-rectennas in the infrared region," in *Proc. Eur. Microw. Conf.*, Oct. 2013, pp. 1–4. [Online]. Available: https://ieeexplore-ieee-org.ezproxy.u-pec.fr/document/6686575
[25] V. Rizzoli, A. Costanzo, D. Masotti, M. Aldrigo, F. Donzelli, and V. Degli-Esposti, "Integration of non-linear, radiation, and propagation CAD techniques for MIMO link design," *Int. J. Microw. Wireless Technol.*, vol. 4, no. 2, pp. 223–232, Apr. 2012.
[26] I. Ibanez-Labiano, S. Nourinovin, and A. Alomainy, "Graphene inkjet-printed ultrawideband tapered coplanar-waveguide antenna on kapton substrate," in *Proc. 15th Eur. Conf. Antennas Propag. (EuCAP)*, Mar. 2021, pp. 1–4, doi: 10.23919/EuCAP51087.2021.9411124.
[27] I. Ibanez-Labiano and A. Alomainy, "Hybrid metal-graphene ultra-wideband antenna," in *Proc. Int. Conf. UK-China Emerg. Technol. (UCET)*, Aug. 2020, pp. 1–3, doi: 10.1109/UCET51115.2020.9205372.
[28] A. Alex-Amor, Á. Palomares-Caballero, E. de la Fuente, A. Muriel-Barrado, J. Valenzuela-Valdés, J. M. Fernández-González, and P. Padilla, "Gain-reconfigurable hybrid metal-graphene printed Yagi antenna for energy harvesting applications," in *Proc. 13th Eur. Conf. Antennas Propag. (EuCAP)*, Mar. 2019, pp. 1–4. [Online]. Available: https://ieeexplore-ieee-org.am.e-nformation.ro/document/8739504
[29] A. Rivadeneyra, J. F. Salmeron, N. Rodriguez, D. P. Morales, R. Colella, F. P. Chietera, and L. Catarinucci, "Laser-fabricated antennas for RFID applications," in *Proc. 50th Eur. Microw. Conf. (EuMC)*, Jan. 2021, pp. 812–815, doi: 10.23919/EuMC48046.2021.9338127.
[30] Z. Hu, S. Jiang, B. Zhang, R. Song, and D. He, "Conformal patch antenna made of graphene-based film for 2.45GHz/5.2GHz frequencies," in *IEEE MTT-S Int. Microw. Symp. Dig.*, Sep. 2020, pp. 1–3, doi: 10.1109/IWS49314.2020.9360071.
[31] H.-R. Zu, B. Wu, Y.-H. Zhang, Y.-T. Zhao, R.-G. Song, and D.-P. He, "Circularly polarized wearable antenna with low profile and low specific absorption rate using highly conductive graphene film," *IEEE Antennas Wireless Propag. Lett.*, vol. 19, no. 12, pp. 2354–2358, Dec. 2020.
[32] J. Li, B. Wu, and C. Fan, "Graphene-based beam steering antenna," in *Proc. IEEE 3rd Int. Conf. Electron. Inf. Commun. Technol. (ICEICT)*, Nov. 2020, pp. 460–462, doi: 10.1109/ICEICT51264.2020.9334372.
[33] J. Perruisseau-Carrier, M. Tamagnone, J. S. Gomez-Diaz, and E. Carrasco, "Graphene antennas: Can integration and reconfigurability compensate for the loss," in *Proc. Eur. Microw. Conf.*, Oct. 2013, pp. 369–372. [Online]. Available: https://ieeexplore.ieee.org/document/6686668

M. ALDRIGO (Member, IEEE) received the Ph.D. degree in electronic engineering, telecommunications, and information technology from the Faculty of Engineering, University of Bologna, Italy, in 2014.

Since 2014, he has been a Principal Researcher III with IMT-Bucharest, Romania. He has coauthored more than 70 papers in ISI-ranked journals and conferences. His main expertise comprises the electromagnetic simulation and experimental characterization of RF/microwave/millimeter-wave/THz systems for wireless/energy-harvesting applications embedding carbon-based, 2-D, and nanoscale ferroelectric materials. He serves or has served as a reviewer for many journals and a (co-)chair in international conferences.

M. DRAGOMAN received the Ph.D. degree in electronics from University ''Politehnica'' Bucharest, Romania, in 1991.

He is currently a Senior Researcher I with IMT-Bucharest, Romania. He has coauthored more than 300 scientific papers in ISI-ranked journals and conferences, and seven monographies.

Prof. Dragoman was awarded the ''Gheorghe Cartianu'' Prize by the Romanian Academy, in 1999. From 1992 to 1994, he was a recipient of the Humboldt Fellowship Award and followed postdoctoral studies at Duisburg University, Germany.

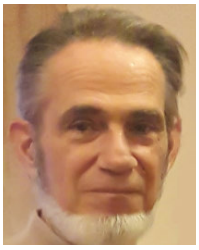

S. IORDANESCU (Life Member, IEEE) was graduated from the Faculty of Electronics and Telecommunications, Polytechnic Institute of Bucharest, Romania, in 1972. He received the Ph.D. degree in electronic engineering from University ''Politehnica'' Bucharest, Romania, in 2000.

From 1972 to 1977, he was with the Institute of Physics and Technology of Radiation Apparatus, Romania. He was a Research Scientist with IMT-Bucharest, Romania, from 1977 to 2000, and a Senior Engineer with Alvarion Romania SRL, from 2000 to 2015. Since 2015, he has been a Senior Researcher with IMT-Bucharest. He is the author of more than 100 scientific papers in peer-reviewed journals and conferences. His research interests include microwave SAW filter and sensor design, the characterization of dielectric and ferroelectric materials, and the design of various microwave and millimeter-wave circuits. He received the ''Tudor Tanasescu'' Romanian Academy Award (with team) for the study ''Micro-machined circuits for microwave and millimeter wave applications—MEMSWAVE,'' in 2003.

A. AVRAM received the B.S. degree in physics and the M.S. degree in plasma physics from the University of Bucharest, in 2009 and 2010, respectively, and the Ph.D. degree in electrical engineering from the ''Politehnica'' University of Bucharest, in 2014.

He is currently a full-time Senior Researcher with IMT-Bucharest, Romania, and the Head of the Laboratory for Carbon-Based Nanotechnologies and Nanostructures. He has experience of over ten years in developing and implementing plasma-assisted processes for etching and deposition of materials, and process integration for the fabrication of micro- and nano-electronic devices and MEMS. Since working as a researcher, he has been actively involved in the implementation of 15 national research projects, one of which he coordinated as a Project Manager. Currently, he is working on the development and integration of carbon-based materials, like graphene derivatives, into different types of sensors for industrial and research applications. His main research interests include developing carbon-based materials and the implementation of fabrication processes for MEMS, microfluidics, micro- /nano-electronics, and dedicated microstructures.

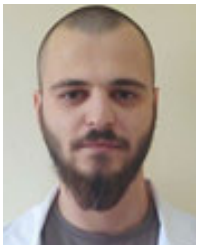

O.-G. SIMIONESCU received the B.S. degree in physics and the M.S. degree from the Faculty of Physics, University of Bucharest, in 2016 and 2018, respectively. He is currently pursuing the Ph.D. degree with the Doctoral School of Physics, University of Bucharest. He is studying carbonic materials' growth processes for sensors and with applications in the field of energy. Since 2016, he has been working as a Physicist with IMT-Bucharest, Romania. He is also working in the field of plasma etching and experimenting with techniques such as reactive ion etching and the Bosch technique. His main research interests include plasma deposition processes such as radiofrequency magnetron sputtering of anti-diffusion layers (i.e., titanium nitride—TiN) and plasma-enhanced chemical vapor deposition of nanocrystalline graphene/graphite, carbon nanotubes, and graphene/graphite nano-walls.

C. PARVULESCU received the Ph.D. degree from the Faculty of Electronics, Telecommunications, and Information Technology, University Politehnica of Bucharest, Bucharest, Romania, in 2015, on the topic ''Micro-nanostructures: Optimized fabrication techniques.''

Currently, he is a Technological Development Engineer III with the Laboratory of Technological Processing, IMT-Bucharest, Romania. He has professional experience in photolithography processes, processing and characterization of photosensitive films, wet etching, nano-imprint lithography processes, bonding processes, microfabrication processes for microfluidics, sensors, opto-microelectronics devices, and microwaves. During his academic career, which started in 2013, he has been holding the M.S. course on ''electronic technologies for optoelectronic applications'' at the Faculty of Electronics, Telecommunications, and Information Technology, University Politehnica of Bucharest. He supervised more than ten master's students. He has coauthored more than 35 papers in international journals and eight national patents. He led/is leading three national projects as a coordinator and participated in more than 25 national projects as a team member.

H. EL GHANNUDI received the Engineering degree in electronic and telecommunication from the University of Tripoli, Libya, in 2002, and the M.S. and Ph.D. degrees in microwave and electronic engineering from the University of Science and Technology of Lille, France, in 2004 and 2007, respectively. During his Ph.D. degree, he worked on the performance of impulse radio ultra-wide band system up converted to the 60-GHz band for high-rate ad-hoc networks. Since 2009, he joined RF Microtech S.r.l., Perugia, Italy, where he is an Associate Member, from 2018. He is currently the Head of the Microwave Systems and Sensor Unit. He has been involved in different European and ESA projects (MEMSPACK, RESKUE). He is also a Coordinator of RF Microtech S.r.l. activities in NANOSMART, NANOPOLY, SMARTEC, and SMARTWAVE H2020 European projects. His research interests include the development and RF design of microwave passive and active components and systems, like RF MEMS, microwave sensors, and RF indoor localization systems.

S. MONTORI received the Ph.D. degree in microwave engineering from the University of Perugia, in 2011. During his Ph.D. degree, he joined the Research Group, Institut für Mikrowellentechnik, Ulm University, directed by Prof. Wolfgang Menzel. Currently, he is the Head of the Antenna Division, RF Microtech S.r.l., Perugia, Italy. His research involvement has resulted in the publication of several papers in the proceedings of international microwave conferences and journals. His research interests include analysis, modeling, and design of phased arrays and reflectarrays, phase-only and phase/amplitude synthesis and optimization techniques for linear, planar, and conformal arrays, design of phase-shifters and passive microwave and millimeter-wave components, and the investigation of innovative architectures for MEMS or diode-based reconfigurable devices. He is a member of the European Microwave Association (EuMA).

L. NICCHI was born in Perugia, Italy, in 1992. He received the B.S. and M.S. degrees in electrical and telecommunications engineering from the University of Perugia, in 2016 and 2019, respectively. He is currently working as an RF Engineer at RF Microtech S.r.l., Perugia, Italy. His research interests include the design and measurements of phased arrays and reflectarrays, antennas for Satcom, and IoT applications.

S. XAVIER received the M.S. degree in thin-layer and surface engineering from the University Louis Pasteur de Strasbourg, France, in 2005, and the Research and Technological Diploma degree from University d'Evry-Val-d'Essonne, France, in 2007. He joined Thales Research and Technology, in 2007, and his specialist field is the development of devices based on carbon nanotubes/2-D materials for RF applications, such as antennas, filters, and switches. He is currently with the Technological and Advanced Characterization Laboratory, where he is responsible for the nano-electronics topics and associated research development. Over the past 14 years, he has been heavily involved in several European and national projects, such as NANORF, NANOSMART, Mercure, NANOCOM, Sims, Gospel, and Opther.

A. ZIAEI (Member, IEEE) received the B.S. degree in electronic engineering from the University of Paris XI, Orsay, in 1997, the M.S. degree in electronic and microwave engineering from the University of Paris VI, Jussieu, in 1998, and the Ph.D. degree in microwaves from the Department of Electronic Engineering, Institut d'Electronique et de Microélectronique et de Nanotechnologie (CNRS-IEMN), in 2005. In 2000, he joined Thales Research and Technology, France, as a Research Engineer. He was involved or in charge of many French or European projects, such as ARHMS, SATURNE, NANOPACK, NANOTEG, NANOTHERM, NANOCOM, NANOTEC, SMARTPOWER, SMARTEC, SMARTHERM, NANOSMART (project coordinator), and NANOPOLY (project coordinator). His research interests include the development, design, fabrication, and characterization of RF MEMS components, such as mechanical switches and transmission lines.